HOSTED BY
ELSEVIER
CrossMark
Available online at www.sciencedirect.com
ScienceDirect
Defence Technology 11 (2015) 229–236
www.elsevier.com/locate/dt

Numerical modeling of friction stir welding using the tools with polygonal pins

M. MEHTA [a], G.M. REDDY [b], A.V. RAO [b], A. DE [c,*]

[a] *Production Engineering Department, BVM Engineering College, Vallabh Vidyanagar, Gujarat, India*
[b] *Defense Metallurgical Research Laboratory, Hyderabad, India*
[c] *Mechanical Engineering Department, IIT Bombay, India*

Received 30 April 2015; revised 5 May 2015; accepted 5 May 2015
Available online 27 May 2015

Abstract

Friction stir welding using the tools with polygonal pins is often found to improve the mechanical strength of weld joint in comparison to the tools with circular pins. However, the impacts of pin profile on the peak temperature, tool torque and traverse force, and the resultant mechanical stresses experienced by the tool have been rarely reported in a systematic manner. An estimation of the rate of heat generation for the tools with polygonal pins is challenging due to their non-axisymmetric cross-section about the tool axis. A novel methodology is presented to analytically estimate the rate of heat generation for the tools with polygonal pins. A three-dimensional heat transfer analysis of friction stir welding is carried out using finite element method. The computed temperature field from the heat transfer model is used to estimate the torque, traverse force and the mechanical stresses experienced by regular triangular, square, pentagon and hexagon pins following the principles of solid mechanics. The computed results show that the peak temperature experienced by the tool pin increases with the number of pin sides. However, the resultant maximum shear stress experienced by the pin reduces from the triangular to hexagonal pins.

Keywords: Friction stir welding; Polygonal tool pin; Aluminum alloy; Numerical model; Tool durability

1. Introduction

The influences of tool shoulder and pin geometry on the microstructure and the tensile properties of the weld joints in friction stir welding (FSW) have been studied extensively [1–5]. The tools with non-circular pin profiles were recently used for FSW with an aim to enhance the flow of the plasticized material and the resulting joint quality [6,7]. The pins with the regular polygonal shapes, such as triangular [8–12], square [13–20], and hexagon [21], and the complex profiles, such as triangular with a convex periphery, circular with three flats, three flutes and four flutes, which are referred to as trivex, triflat, triflute and quadflute, respectively, are considered [6,7,10]. The pin profiles with the regular polygon shape are preferred in comparison to the complex non-circular shapes because of the ease of manufacturing of the former ones. The relative performance and the longevity of the tools with circular and non-circular pins during FSW were also reported recently [22]. Although many of these studies have indicated the improved performance of the tools with the polygonal pins in comparison to the circular pins, the influences of the polygonal pin cross-section on the peak temperature, and tool torque and forces have been rarely studied using a quantitative numerical model.

Colegrove et al. reported that the Trivex pin profile could prevent material entrapment and reduce shearing force on the advancing side of the pin, resulting in lesser pin traverse force compared to the Triflute pin profile [6]. In subsequent studies, Colegrove, et al. found the Triflat pin to produce the best welds followed by the Triflute and Trivex profiles although the

* Corresponding author.
E-mail address: amit@iitb.ac.in (A. DE).
Peer review under responsibility of China Ordnance Society

http://dx.doi.org/10.1016/j.dt.2015.05.001

Triflat pin increased the total torque [7] and [8]. Fujii et al. reported greater joint strength in FSW of AA5083 using the tool pins with triangular cross-section at a rotational speed of 1500 rpm and at varying weld pitch compared to a circular pin profile[12]. The tool pins with square cross-section provided the best mechanical properties of weld joint for a range of welding conditions in FSW of SiC reinforced AA1050 [13], AA6061 [14] and [15], Al-10 wt.% TiB_2 MMC [16], AA2219 [19] and [20], and in dissimilar materials of AA5083 and AA6351 [18] compared to the other pin profiles. Amongst the pins with several polygonal cross-sections, a typical hexagonal pin profile provided superior tensile properties of weld joint in FSW of AA2014 although the joint properties obtained with the square, pentagon and hexagonal pins did not show any significant variation [21]. Most of these studies on FSW with polygonal pin profiles concentrated on the testing and characterization of the final weld joints.

The present work depicts the development of a three-dimensional heat transfer analysis of FSW process following a novel methodology to analytically estimate the rate of heat generation for tools with polygonal pins shapes. The area of contact between the flat faces of polygonal pins and the plasticized material is estimated based on the principles of orthogonal machining [22]. A three-dimensional steady state heat transfer model of FSW process is developed using finite element method to compute the temperature fields in the workpiece and the tool pin. The computed temperature distribution of the workpiece material surrounding the tool is used to analytically estimate the torque and traverse force experienced by the tool. The computed values of thermal cycle, torque and traverse force are validated with the corresponding experimentally measured results for FSW of AA2014-T6. The estimated values of the pin traverse force are used to compute the stresses on polygonal pin profiles based on the principles of solid mechanics.

2. Experimental study

300 mm (length) × 100 mm (width) × 5 mm (thickness) aluminum alloy (AA2014-T6) plates are welded by friction stir welding in square butt joint configuration using EN40 tools with constant shoulder diameter of 12 mm and pin length of 4.7 mm. The rotational and linear speeds, the axial pressure and the tool tilt angle are kept constant for all the welds, which are 1000 rpm, 7.73 mm/s, 90 MPa and 2°, respectively. Four different tool pins with triangular, square, pentagon and hexagon profiles are used. Since the pins are tapered along the length, the side lengths of each pin profile at the root and at the tip are different (Table 1). The circumcircle diameters of all the polygonal pins are 6 mm and 3.6 mm at the root and at the tip, respectively. Table 2 depicts the compositions of the workpiece and the tool materials [23] and [24]. Table 3 provides the thermophysical properties of the workpiece material [25]. The density, specific heat and thermal conductivity of the tool material are considered as 7850 kg/m^3, 485.34 J/(kg·K) and 34.73 W/(m·K), respectively [25]. The transient thermal cycles are measured using K-type thermocouples during the actual FSW experiments with a transverse distance of 4 mm from the original weld joint interface and at a depth of 2 mm from the top surface. The torque and the traverse force are also measured during the actual FSW process.

Table 1
Tool pin geometry.

Regular polygon pin profile	Pin side length/mm	
	Root	Tip
Triangular	5.19	3.11
Square	4.24	2.54
Pentagon	3.52	2.11
Hexagon	3.0	1.8

3. Theoretical formulation

A steady state three-dimensional heat conduction analysis of the FSW process is carried out with the governing differential equation

$$\frac{\partial}{\partial x}\left(k\frac{\partial T}{\partial x}\right)+\frac{\partial}{\partial y}\left(k\frac{\partial T}{\partial y}\right)+\frac{\partial}{\partial z}\left(k\frac{\partial T}{\partial z}\right)+\dot{Q}=\rho C U_1\frac{\partial T}{\partial x} \quad (1)$$

where ρ, k, C and U_1 refer to the density, thermal conductivity, specific heat, and the constant welding speed, respectively; and T is the temperature variable. The term $\dot{Q}$ accounts for the rate of internal heat generation per unit volume. The rate of the frictional heat generation per unit area (q_S) at the tool–workpiece interface is applied as a surface flux and estimated as [26,27]

$$q_S=\eta_h\times\left[\eta_m(1-\delta)\tau_y+\delta\mu_f P_N\right](\omega r-U_1\sin\theta) \quad (2)$$

where η_h is the fraction of heat transferred to workpiece; η_m depicts the fraction of mechanical work due to sticking friction converted to heat; P_N is the axial pressure; τ_y is the temperature-dependent shear yield stress of deformed material; r is the radial distance from tool axis; θ is the orientation of the point from the welding direction; ω is the angular speed; and, δ and μ_f refer to the local variations in fractional sliding and the coefficient of friction, respectively. A symmetric analysis is undertaken considering the plane of symmetry along the original weld joint interface. The rate of heat generation along the pin − workpiece interface is applied as a volumetric heat input by multiplying q_S by A_i/V_i where A_i and V_i refer respectively to the surface area and volume of the i-th discrete element adjacent to the tool pin surface [26,27]. A temperature-dependent convective heat transfer coefficient as $h_b\times(T-T_0)^{0.25}$ is applied along the bottom surface, where

Table 2
Composition of workpiece [23] and tool material [24].

AA2014-T6 (Workpiece)	Element	Al	Cu	Si	Mn	Mg
	wt./%	90.4–95.0	3.9–5.0	0.5–1.2	0.4–1.2	0.2–0.8
EN40 (Tool)	Element	C	Mn	Si	Cr	Mo
	wt./%	0.3–0.5	0.4–0.8	0.1–0.35	2.5–3.5	0.7–1.2

Table 3
Thermophysical properties of the workpiece material [25].

Solidus temperature/K; Density/(kg·m^{-3})	780.15; 2800.0
Specific heat/(J·kg^{-1} K^{-1})	$426.576 + 2.492T - 4.25 \times 10^{-3}T^2 + 2.7245 \times 10^{-6}T^3$ for $T \leq 813$ K 1108.0 for $T > 813.15$ K
Thermal conductivity/(W·m^{-1}K^{-1})	$50.738 + 0.6904T - 1.1 \times 10^{-3}T^2 + 5.4295 \times 10^{-7}T^3$ for $T \leq 473.15$ K 188.65 for $T > 473.15$ K
Yield strength/MPa	$((414.759 - 33.6086)/(1 + \exp((T - 433.248)/23.3938))) + 33.6086$ for 297 K $\leq T \leq$ 911 K

h_b equals to 0.0007 W/(m^2·K$^{1.25}$) and T_0 is the ambient temperature [28]. The mechanical heating due to the viscous dissipation of the deformed material around the pin is neglected as the velocity gradient in the shear layer could not be estimated in the conduction heat transfer model.

In contrast to the pins with circular cross-section, the pins with polygonal profiles in FSW exhibit the flat faces and the associated edges. As a result, the estimation of the length of contact between the tool pin side and plasticized material, which is needed to estimate the rate of heat generation along the pin sides, becomes difficult. This is accomplished by considering the faces and the edges of the polygonal tool pins in FSW, which are analogous to the rake face and the cutting edge of a typical cutting tool in machining.

The chips in machining experience plastic deformation and shear fracture along a plane that is inclined at an angle α, which is known as shear angle and estimated as [22,29,30]

$$\alpha = (\pi/4) + \beta - \gamma \tag{3}$$

where γ is the mean friction angle along tool–chip interface, $\tan\gamma \approx 0.5$; and β is the rake angle that depicts the inclination of the tool rake surface with the normal to the tangential velocity vector at the cutting edge. The chip-tool contact length in machining is estimated, presuming that the boundary of plasticized chip region meets the rake face at 45^0 [22,29,30]

$$S = t \times [1 + \tan(\alpha - \beta)] = t \times [1 + \tan(\pi/4 - \gamma)] = 4t/3 \tag{4}$$

where t is the deformed chip thickness. Eq. (4) can therefore be used to estimate the length of contact between each pin side of the polygonal tool and plasticized material in FSW. In case of FSW, the thickness t of the deformed chip matches the layer thickness of the plasticized material around the pin and can be estimated as [22]

$$t = c - i + p \tag{5}$$

where c and i are the circumradius and inradius of the regular polygon pin profile, respectively; and p is the weld pitch, i.e. the linear distance travelled by the pin in each revolution. The net contact length between the pin surface-plasticized material can therefore be estimated as [22]

$$S \times N = \frac{4}{3}(c - i + p) \times N \tag{6}$$

Fig. 1(a)–(d) schematically show the pin side length (H) at the root, the stick length (S) per pin side and the rake angle (β) for tool pins with triangular, square, pentagon and hexagonal cross-sections. A comparison of Fig. 1(a)–(d) depicts a decrease in stick length (S) and an increase in the rake angle (β) with the increase in the number of pin sides. It is clear from Fig. 1(a)–(d) that the rake angles for the regular triangular, square, pentagon and hexagon pin profiles are $-30°$, $-45°$, $-54°$ and $-60°$, respectively.

The torque (M) and traverse force (F) on the tool are estimated analytically from the numerically computed temperature field by considering the corresponding mechanical properties of the deforming material adjacent to the tool [26,27]

$$\begin{aligned} M = &\int_{R_P}^{R_S} r\left[(1-\delta)\tau_y + \delta\mu_f P_N\right] \times (2\pi r \mathrm{d}r) + \int_0^L r\left[(1-\delta)\tau_y \right. \\ &\left. + \delta\mu_f \sigma_y\right] \times (2\pi r \mathrm{d}l) + \int_0^{R_P} r\left[(1-\delta)\tau_y + \delta\mu_f P_N\right] \\ &\times (2\pi r \mathrm{d}r) \end{aligned} \tag{7}$$

$$\begin{aligned} F = &\int_{R_P}^{R_S} \left[(1-\delta)\tau_y + \delta\mu_f P_N\right] \times (2\pi r \mathrm{d}r) \\ &+ \int_0^L \sigma_y \times \mathrm{d}A + \int_0^{R_P} \left[(1-\delta)\tau_y + \delta\mu_f P_N\right] \times (2\pi r \mathrm{d}r) \end{aligned} \tag{8}$$

In Eqs. (7) and (8), the first term accounts for the contribution by tool shoulder interface, and the second and the third terms are contributed from the side and the bottom surfaces of the pin, respectively. Eqs. (7) and (8) are evaluated using Newton-Cotes closed integration technique with seven segments.

During FSW, the tool pin experiences a combined bending and torsion due to the simultaneous translational and rotational motions through the plasticized workpiece material. As a result, the pin will experience normal stress σ_B and shear stress τ_B due to bending and shear stress τ_T due to torsion. The normal stress σ_B due to bending at any point on a pin profile is estimated as [26,27]

$$\sigma_B = \frac{M_y\, x}{I_{yy}} = \frac{x}{I_{yy}} \int_{z_1}^{L} z\, q(z)\, \mathrm{d}z \tag{9}$$

where M_y represents the maximum bending moment; x is the normal distance of the point of interest from the neutral axis; I_{yy} is the second moment of area; L represents the pin length; z_1 is the distance of the point of interest from the shoulder, $q(z)$

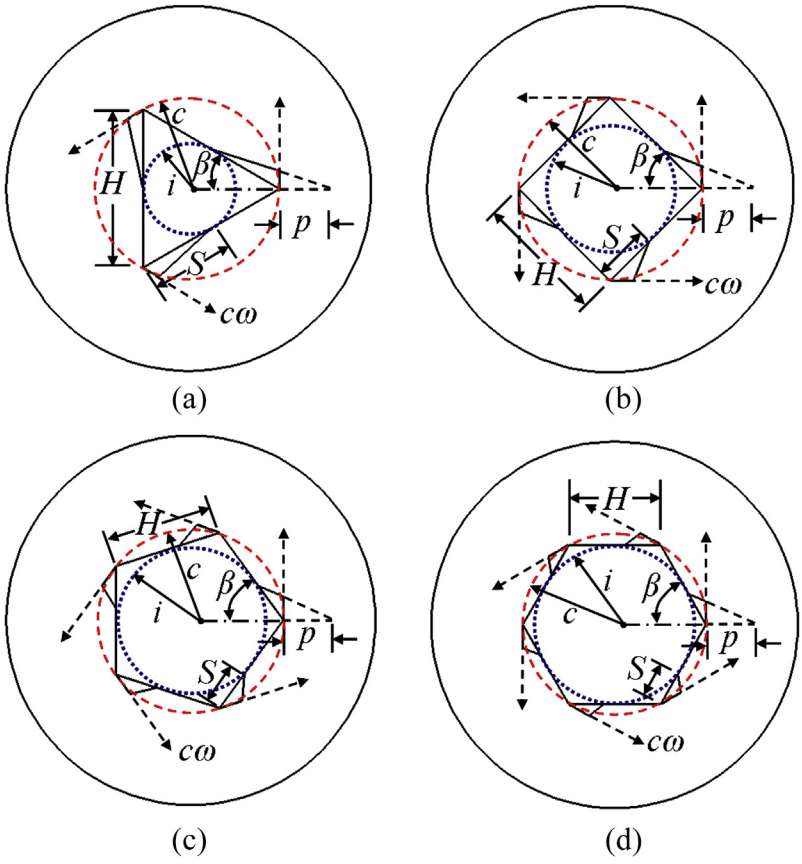

Fig. 1. Schematic diagram of the regular polygon pin depicting the shoulder (outer circle), pin side length (H), stick length (S), tangential velocity vector of plasticized material ($c\omega$) and the rake angle (β) for regular (a) triangular, (b) square, (c) pentagon and (d) hexagon pins. Blue dotted and red dashed lines indicate incircle and circumcirle, respectively.

is the force per unit length acting on a differential element of length dz at a distance (z_1+z) from the shoulder. The shear stress τ_B due to bending is estimated as [26,27]

$$\tau_B = \frac{VQ}{I_{yy}g} = \frac{Q}{I_{yy}g}\int_{z_1}^{L} q(z)\,\mathrm{d}z \tag{10}$$

where V is the maximum shear force; Q is the first moment of area of the section about the neutral axis (N.A.); and g is the length of a segment through the point of interest and parallel to the neutral axis. The term Q is estimated as the product of the area of the section away from the N.A. and the normal distance from the centroid of the area to the N.A. The shear stress τ_T due to torsion occurs at the mid-points of the pin sides and is estimated for the triangular [31], square [32] and [33], pentagon [34] and hexagon [35] pin profiles following Eqs.11–14, respectively

$$\tau_T = \frac{20 \times M_T}{H^3} \tag{11}$$

$$\tau_T = \frac{M_T}{0.208 \times H^3} \tag{12}$$

$$\tau_T = \frac{1.9721 \times M_T}{H^3} \tag{13}$$

$$\tau_T = \frac{M_T}{0.9765 \times H^3} \tag{14}$$

where M_T refers to the sticking torque experienced by the tool pin; and H is the pin side length at the root. The resultant maximum shear stress, τ_{max}, on a pin profile can finally be estimated following the Tresca's yield criteria as [26,27]

$$\tau_{max} = \sqrt{\left(\frac{\sigma_B}{2}\right)^2 + (\tau_B + \tau_T \cos\lambda)^2 + (\tau_T \sin\lambda)^2} \tag{15}$$

where λ is the angle between τ_T and τ_B, measured in anti-clockwise direction from τ_B to τ_T. The stresses at any point on a regular polygon pin profile would depend on the location of the point, the pin cross-section and its orientation during one complete rotation. Hence, τ_{max} is estimated at all the locations where one of σ_B, τ_B and τ_T would reach the maximum during one complete rotation and the maximum value of τ_{max} is considered for each polygonal pin.

The numerical model is developed using the commercial finite element software, ABAQUS (version 6.8EF-1). The solution domain is discretized using three-dimensional eight

node brick elements (DCC3D8 in ABAQUS) with the temperature as the nodal degrees of freedom. A finer mesh is used near to and around the tool and is coarsened progressively away from the tool. Four user-defined subroutines – DFLUX, FILM, USDFLD and UMASFL – in ABAQUS are used to assign respectively the non-uniform heat flux along the tool–workpiece interface, the convective heat transfer coefficient at the bottom surface, the tool pin properties and the mass velocity to the workpiece with respect to the heat source.

4. Results and discussion

Fig. 2(a) depicts the computed temperature distribution during FSW of AA2014-T6 using a regular triangular pin. The region heated above 600 K, which is nearly 0.8 times the solidus temperature of the workpiece material, is represented in red color and presumed to be the softened zone to primarily experience the traction by the rotational motion of the tool pin. The size of the high temperature region is wider underneath the shoulder and tends to reduce along the length of the pin in the thickness direction. This can be attributed to higher rate of frictional heat generation along the shoulder-workpiece interface in comparison to the same around the surfaces of the tool pin. The rate of frictional heat generation on the vertical surface of the pin is slightly higher than that on the bottom surface due to larger surface area of the former. Similarly, Fig. 2(b)–(d) depict the computed temperature distributions for the regular square, pentagon and hexagon pins, respectively. A comparison of Fig. 2(a)–(d) depicts an increase in the high temperature region, which is above 600 K, in the vicinity of the pin vertical surface with the increase in the number of pin sides that is attributed to the increase in the rate of frictional heat generation along the pin vertical and bottom surfaces.

Fig. 3(a)–(d) depict a comparison between the numerically computed and experimentally measured thermal cycles during FSW of AA2014-T6 using a regular triangular, square, pentagon and hexagon pins, respectively. The increase in the peak temperature from the triangular pin profile towards the hexagon pin profile is attributed to the enhanced rate of frictional heating around the pin vertical and bottom surfaces with the increase in the number of pin sides. Overall, a fair agreement between the computed and corresponding measured thermal cycles can be noted in Fig. 3. The slight deviation between the computed and corresponding measured thermal cycles may be attributed to the neglect of heating due to mechanical deformation and the presumed thermophysical properties of AA2014-T6 (Table 3). Fig. 4 depicts the variation in the computed peak temperature for four different regular polygonal pins. It is noted that the peak temperature increases with the increase in the number of pin sides from the triangular pin to the hexagon pin. Higher number of pin sides increases the overall pin-workpiece contact area, resulting in greater rate of frictional heat generation, in particular, on the pin vertical surfaces, which leads to a higher peak temperature.

Fig. 5(a) and (b) depict a comparison between the analytically estimated and corresponding experimentally measured torques and traverse forces, respectively, for four different regular polygonal pins. The total torque remains nearly unchanged while the traverse force decreases with the increase in the number of sides from the triangular pin to hexagon pin. For a given shoulder diameter and pin circumradius (c), the increase in the number of pin sides reduces the shoulder-workpiece contact area while increases the pin-workpiece contact area, resulting in a nearly steady tool torque. However, the increase in the number of pin side enhances the rate of frictional heat generation and the resulting softening of a greater amount of deformed material around the pin surfaces, leading to the decrease in traverse force. A fair agreement

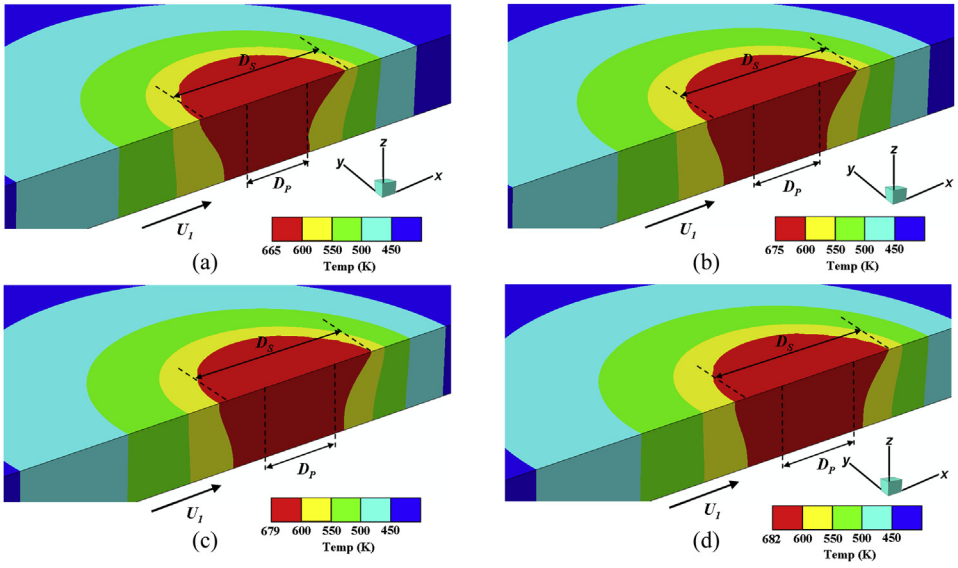

Fig. 2. Computed temperature fields during FSW of AA2014-T6 with (a) triangular, (b) square, (c) pentagon and (d) hexagon tool pins at a rotational speed of 1000 rpm and the welding speed of 7.73 mm/s. D_S and D_P refer to the shoulder and pin diameters, respectively.

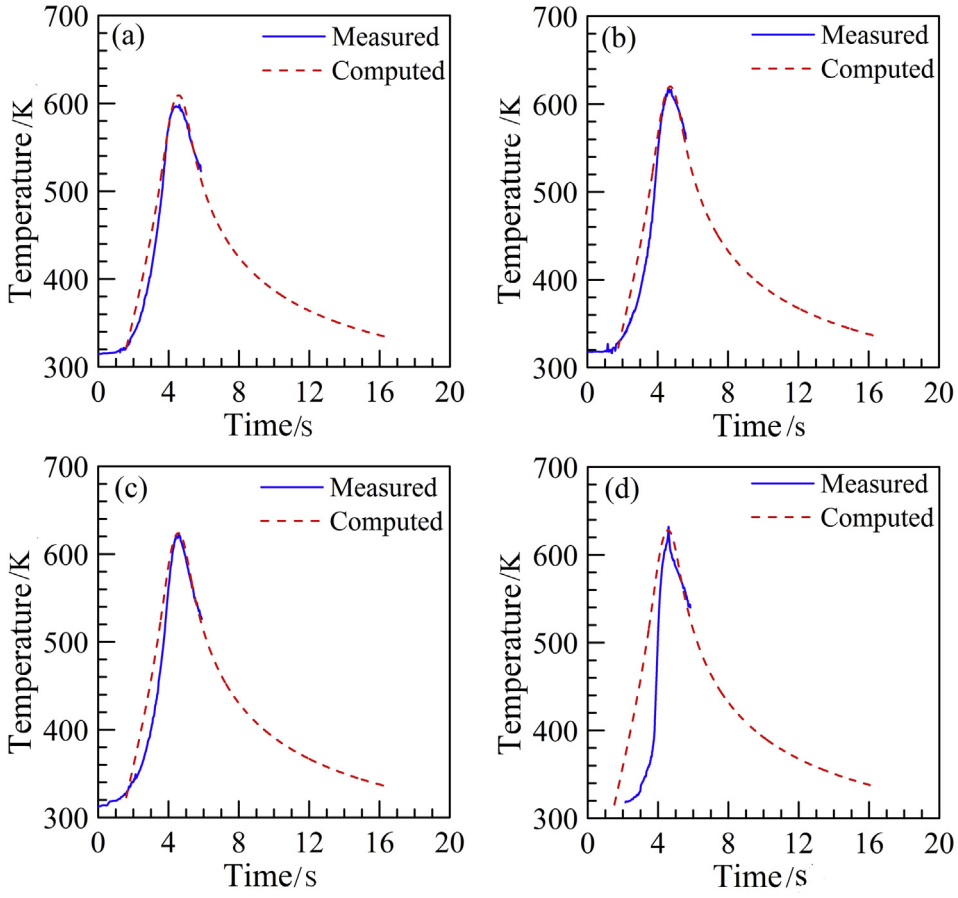

Fig. 3. The comparison of the computed and corresponding measured thermal cycles at 4 mm away from the original weld joint interface and 2 mm from the workpiece top surface in FSW of AA2014-T6 with (a) triangular, (b) square, (c) pentagon and (d) hexagon pins.

between the computed and corresponding measured torques and traverse forces for various regular polygonal pins can be noted in Fig. 5.

Fig. 6(a) depicts the estimated variations in the components of mechanical stresses (σ_B, τ_B, τ_T and τ_{max}) experienced by

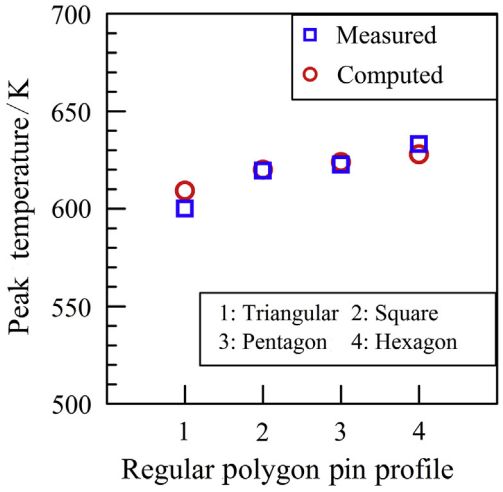

Fig. 4. Comparison of the computed and corresponding measured peak temperatures at 4 mm away from the original weld joint interface and 2 mm from the workpiece top surface during FSW of AA2014-T6 with four different polygonal pins.

FSW tool with triangular pin at different orientations (ξ) during one complete rotation. The values of σ_B, τ_B, τ_T and τ_{max} at 30° are estimated for the regular triangular pin, as indicated in the plot of τ_{max} for clarity. The analytically evaluated values of σ_B, τ_B, τ_T and τ_{max} indicate the apparent trend of the component of stresses during one complete rotation of the tool. Fig. 6(a) shows that τ_T is constant for all values of ξ while σ_B is the highest and lowest at $\xi = 60°$ and 240°, respectively, and τ_B assumes multiple occurrences of low and high values during one complete rotation of the tool pin. The resultant maximum shear stress, τ_{max}, is the highest at $\xi = 120°$ and 180° where τ_B is at its maximum and the component of τ_T along τ_B is in the same direction as that of τ_B. In contrast, τ_{max}, is the minimum at $\xi =$ zero and 300° where τ_B is also the maximum while the component of τ_T along τ_B is in the opposite direction as that of τ_B. The estimated maximum value of τ_{max} is 581.76 MPa for the regular triangular pin. Fig. 6(b) depicts the estimated results of the largest magnitude in τ_{max} for four different regular polygonal pins for the welding conditions considered here. The largest magnitude of τ_{max} reduces from the triangular pin profile to the hexagon pin profile, which is attributed to the enhanced structural stiffness and the decrease in traverse force with an increase in the number of pin sides.

The numerically computed values of the peak temperature and the analytically estimated values of the maximum shear

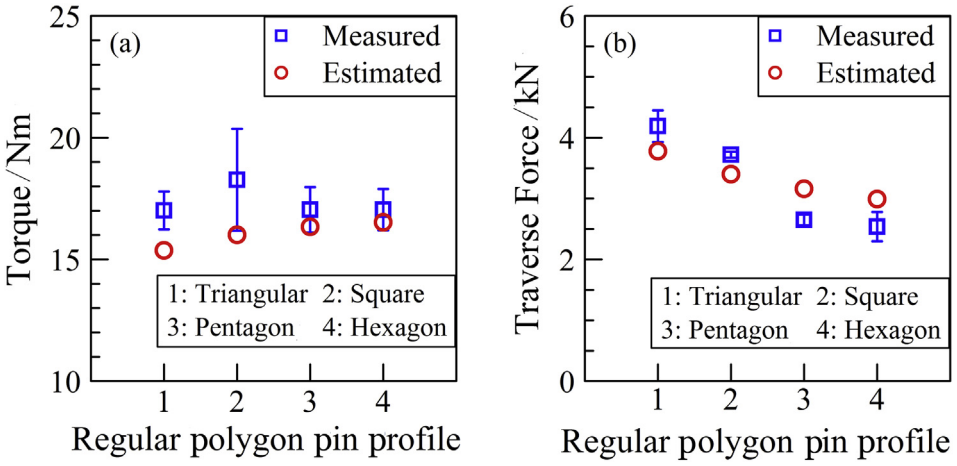

Fig. 5. Comparison of the analytically estimated and corresponding measured (a) torques and (b) traverse forces during FSW of AA2014-T6 with different polygonal pins.

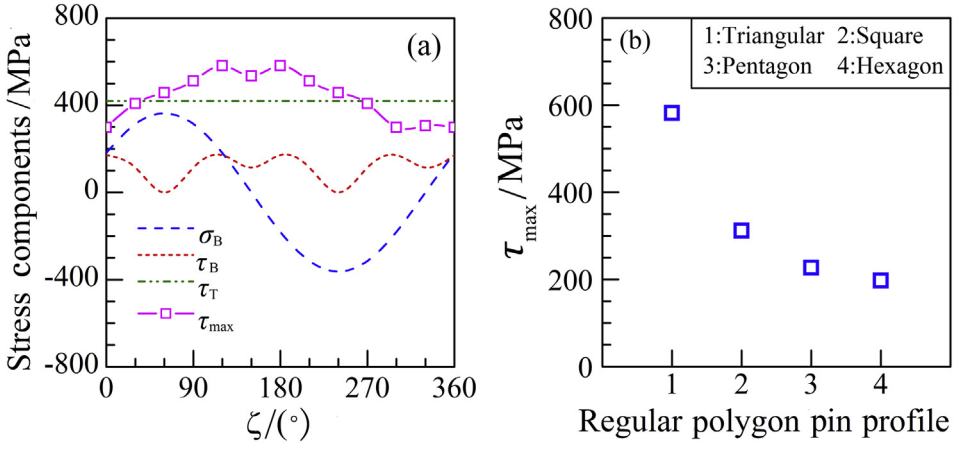

Fig. 6. (a) Estimated variations in components of mechanical stresses (σ_B, τ_B, τ_T) and resultant maximum shear stress (τ_{max}) on pin side at different orientations (ξ) during one complete rotation of a triangular pin for FSW of AA2014-T6, and (b) estimated values of maximum τ_{max} for four different regular polygon pins during FSW of AA2014-T6.

stress, τ_{max}, can be used further to provide an assessment of the longevity of the FSW tools with polygonal pin shapes. A tool durability index is therefore presumed here as the ratio of the shear yield strength of the tool pin material at the computed peak temperature and τ_{max} experienced by the corresponding pin. Thus a tool pin with a higher value of durability index is expected to be lesser susceptible to premature failure during actual FSW operation. For example, the peak temperature and τ_{max} experienced by the triangular pin are estimated as 662 K and 581.76 MPa, respectively, for the welding conditions considered here. The corresponding durability index can therefore be estimated as (615.0/581.76) where 615 MPa is the shear yield strength of tool pin material at 662 K [25]. The estimated values of τ_{max} experienced by the square, pentagon and hexagonal pin profiles are 311.99 MPa, 226.70 MPa and 197.31 MPa, respectively, with the corresponding peak temperatures of 672 K, 676 K and 680 K. The tool durability indices are therefore estimated as 1.96 (611/311.99), 2.69 (609/226.70) and 3.08 (607/197.31), respectively, for the square, pentagon and hexagon pin profiles. Thus the hexagon pin profile depicts the maximum durability index and would be least susceptible to premature fracture for the welding conditions considered here [29]. The estimated values and the general trend of the tool durability indices provide a first step towards the fail-safe design of FSW tool following mechanics-based principle, which is currently absent. However, the further studies need to also consider the possible vibration of tool during actual FSW operation for the estimation of a more practical tool durability index.

5. Conclusions

The present work outlines a novel approach to estimate the rate of frictional heat generation by polygonal pins in friction stir welding based on the principle of orthogonal machining. For a given welding condition, the regular triangular and hexagon pins experience the largest and smallest magnitudes of the resultant maximum shear stress, respectively. The decrease in the resultant maximum shear stress from the triangular pin profile to the hexagon pin profile can be

attributed to the decrease in traverse force and the enhanced structural stiffness with an increase in the number of pin sides and the resulting reduction in the bending moment and shear force. The increase in the section modulus enhances the structural stiffness of the hexagon pin profile to aid higher resistance against the shear stress due to bending, which appears to have the predominant influence on the resulting maximum shear stress experienced by the pin profiles.

References

[1] Thomas WM, Nicholas ED. Friction stir welding for the transportation industries. Mater Des 1997;18:269−73.

[2] Rowe CED, Thomas WM. Advances in tooling materials for friction stir welding. Technical report. Cambridge, UK: TWI; 2005.

[3] Rai R, De A, Bhadeshia HKDH, DebRoy T. Review: friction stir welding tools. Sci Technol Weld Join 2011;16:325−42.

[4] Threadgill PL, Leonard AJ, Shercliff HR, Withers PJ. Friction stir welding of aluminum alloys. Int Mater Rev 2009;54:49−93.

[5] Nandan R, DebRoy T, Bhadeshia HKDH. Recent advances in friction-stir welding − process, weldment structure and properties. Prog Mater Sci 2008;53:980−1023.

[6] Colegrove PA, Shercliff HR. Development of Trivex friction stir welding tool Part 1 − two-dimensional flow modeling and experimental validation. Sci Technol Weld Join 2004;9:345−51.

[7] Colegrove PA, Shercliff HR. Two-dimensional CFD modeling of flow round profiled FSW tooling. Sci Technol Weld Join 2004;9:483−92.

[8] Colegrove PA, Shercliff HR. CFD modeling of friction stir welding of thick plate 7449 aluminium alloy. Sci Technol Weld Join 2006;11:429−41.

[9] Zettler R, Lomolino S, dos Santos JF, Donath T, Beckmann F, Lippman T, et al. Effect of tool geometry and process parameters on material flow in FSW of an AA2024-T351 alloy. Weld World 2005;49:41−6.

[10] Hattingh DG, Blignault C, van Niekerk TI, James MN. Characterization of the influences of FSW tool geometry on welding forces and weld tensile strength using an instrumented tool. J Mater Process Technol 2008;203:46−57.

[11] Lorrain O, Favier V, Zahrouni H, Lawrjaniec D. Understanding the material flow path of friction stir welding process using unthreaded tools. J Mater Process Technol 2010;210:603−9.

[12] Fujii H, Cui L, Maeda M, Nogi K. Effect of tool shape on mechanical properties and microstructure of friction stir welded aluminum alloys. Mater Sci Eng A 2006;419:25−31.

[13] Mahmoud ERI, Takahashi M, Shibayanagi T, Ikeuchi K. Effect of friction stir processing tool probe on fabrication of SiC particle reinforced composite on aluminum surface. Sci Technol Weld Join 2009;14:413−25.

[14] Elangovan K, Balasubramanian V, Valliappan M. Influences of tool pin profile and axial force on the formation of friction stir processing zone in AA6061 aluminium alloy. Int J Adv Manuf Technol 2008;38:285−95.

[15] Elangovan K, Balasubramanian V. Influences of tool pin profile and tool shoulder diameter on the formation of friction stir processing zone in AA6061 aluminium alloy. Mater Des 2008;29:362−73.

[16] Vijay SJ, Murugan N. Influence of tool pin profile on the metallurgical and mechanical properties of friction stir welded Al−10wt.% TiB2 metal matrix composite. Mater Des 2010;31:3585−9.

[17] Sundaram NS, Murugan N. Tensile behavior of dissimilar friction stir welded joints of aluminum alloys. Mater Des 2010;31:4184−93.

[18] Palanivel R, Mathews PK, Murugan N, Dinaharan I. Effect of tool rotational speed and pin profile on microstructure and tensile strength of dissimilar friction stir welded AA5083-H111 and AA6351-T6 aluminum alloys. Mater Des 2012;40:7−16.

[19] Elangovan K, Balasubramanian V. Influences of pin profile and rotational speed of the tool on the formation of friction stir processing zone in AA2219 aluminium alloy. Mater Sci Eng A 2007;459:7−18.

[20] Elangovan K, Balasubramanian V. Influences of tool pin profile and welding speed on the formation of friction stir processing zone in AA2219 aluminium alloy. J Mater Process Technol 2008;200:163−75.

[21] Ramanjaneyulu K, Reddy GM, Rao AV, Markandeya R. Structure-property correlation of AA2014 friction stir welds: role of tool pin probe. J Mater Eng Perform 2013;22:2224−40.

[22] Mehta M, De A, DebRoy T. Material adhesion and stresses on friction stir welding tool pins. Sci Technol Weld Join 2014;19:534−40.

[23] Henry SD. ASM speciality handbook: aluminum and aluminum alloys. Materials Park, OH: ASM International; 1993. p. 658−62.

[24] Woolman J, Mottram RA. The mechanical and physical properties of the British standard: En steels (B.S. 970-1955) − volume 3 (En 40 to En 363). Oxford: Pergamon Press Limited; 1969.

[25] Smithells CJ. Smithells metal reference book. London: Butterworths; 1983.

[26] Arora A, Mehta M, De A, DebRoy T. Load bearing capacity of tool pin during friction stir welding. Int J Adv Manuf Technol 2012;61:911−20.

[27] Mehta M, Arora A, De A, DebRoy T. Tool geometry for friction stir welding − optimum shoulder diameter. Metall Mater Trans A 2011;42A:2716−22.

[28] Nandan R, Roy GG, Lienert TJ, DebRoy T. Three-dimensional heat and material flow during friction stir welding of mild steel. Acta Mater 2007;55:883−95.

[29] Boothroyd G, Knight WA. Fundamentals of machining and machine tools. Florida: Taylor and Francis Group; 2006.

[30] Chattopadhyay AB. Machining and machine tools. New Delhi: Wiley India Pvt. Ltd; 2000. p. 84−115.

[31] Srinath LS. Advanced mechanics of solids. New Delhi: Tata McGraw-Hill; 2003.

[32] Timoshenko SP, Goodier JN. Theory of elasticity. Singapore: McGraw-Hill book company; 1970.

[33] Sadd MH. Elasticity − theory, applications, and numerics. Oxford: Elsevier Butterworth Heinemann; 2005.

[34] Kovar A. Moment tuhosti v krouceni pravidelneho petiuuhelnika (Torsion rigidity moment of the regular pentagon). Appl Math 1957;2:58−65.

[35] Timoshenko S. Strength of materials: Part 2 − advanced theory and problems. New Delhi. 2002.